

A STATISTICAL ANALYSIS OF PATCHES OF OCEANIC SMALL-SCALE ACTIVITY

Instruments that sample oceanic temperature and conductivity either by acquiring vertical profiles at a single horizontal location or by making horizontal tows using sparsely instrumented arrays have traditionally lacked enough horizontal or vertical resolution to characterize simultaneously the full two-dimensional structure of patches of small-scale activity associated with oceanic turbulence. APL has recently developed a thermistor array with very high vertical resolution that has significant advantages for studying the geometric structure of ocean patches. In this article, a methodology is presented for detecting patches and quantifying their vertical and horizontal scales by exploiting the high vertical resolution of the array. Preliminary results of an analysis of 200 kilometers of data are consistent with previous observations of patches associated with diffusive instabilities as well as with other generation mechanisms.

INTRODUCTION

In the ocean, fluid motions and associated variations in conductivity and temperature exhibit a wide range of spatial and temporal scales. Large-scale motions with time scales of hours to years are associated with large-scale synoptic flows, oceanic fronts, and internal waves. Small-scale motions with time scales of hours to minutes and length scales from tens of meters to centimeters are associated with oceanic turbulence and temperature finestructure or microstructure. The interaction of flows on these two disparate scales (in particular, how energy is transferred from large-scale motions to small-scale motions and is dissipated as turbulence) is of great interest to oceanographers. To understand this energy transport, it is necessary to quantify the spatial and temporal scales of mixing events in the ocean.

When sampled by a towed or dropped instrument, the signature of oceanic turbulence is small-scale (or high-frequency) variations in velocity, temperature, and conductivity. These signatures, commonly called microstructure or small-scale activity (SSA), have been observed in the ocean for decades, and the oceanographic literature abounds with examples of such mixing events.¹⁻⁷ Temperature and conductivity fluctuations with length scales of a few centimeters to a meter tend to occur in patches that are typically 1 to 10 meters thick and extend for hundreds of meters horizontally. These patches are manifestations of various mechanisms that transport energy from large-scale flows into turbulence. The horizontal and vertical scales of these patches provide information on the relative importance of the various mechanisms for generating turbulence in the ocean.^{4,6,7} Generation mechanisms include double diffusive instabilities, shear instabilities, and internal wave breaking.

The occurrence of double diffusive instabilities (also called salt-fingering) takes place because heat and salt diffuse at different rates. When hot salty water lies above cool fresh water, an instability can arise even though the lighter (less dense) fluid is above the denser fluid. A small perturbation of the interface causes heat to diffuse relatively rapidly between the two fluids while their salt content changes only slightly. Thus a cool fluid parcel that is displaced upward warms rapidly because of the surrounding warm water. However, since the salinity of the parcel is low, it is lighter than the surrounding fluid and continues to rise. This mechanism gives rise to long, thin, vertical columns of cells of similar salinity, known as salt fingers, that are sources of SSA on conductivity and temperature sensors. More details of this mechanism are found in Ref. 7.

Shear instabilities are a consequence of ocean currents that have a strong vertical spatial gradient relative to the ambient density stratification. When two water masses with differing horizontal currents overlay each other, the interface between the two becomes unstable and "rolls up," creating a billow pattern. The force that tends to prevent this mixing is the ambient stratification. The criterion for mixing is that a non-dimensional parameter known as the Richardson number be less than $1/4$:⁸

$$Ri = \frac{N^2}{(du/dz)^2} < \frac{1}{4},$$

where N is the buoyancy frequency based on the density profile $\rho(z)$,

$$N^2 = \frac{-g}{\rho} \frac{d\rho}{dz},$$

and du/dz is the change in horizontal currents with depth. We see that mixing can occur when the shear is strong and/or the stratification weak (small value of N). The shear can result from interleaving currents, from large internal waves, or from boundary effects. The breaking of internal waves can also cause regions of mixing and SSA.

Although the literature abounds with examples of patches of SSA from ocean measurements, simultaneous statistical characterizations of the horizontal and vertical extents of these patches are relatively rare. This is primarily due to limitations imposed by the instrumentation used to study these phenomena. Most measurements of microstructure have been made using dropped instruments such as CTDs (probes of conductivity, temperature, depth), which produce high-resolution vertical profiles of temperature and conductivity. Although horizontal information can be acquired by repeated casts of the CTD probes at different horizontal locations, it is difficult and time-consuming to gather enough data by this method to perform a statistical characterization of the two-dimensional SSA field. In contrast, a vertical array of instruments such as a thermistor chain, towed horizontally, can produce efficiently and quickly many kilometers of well-resolved horizontal data. However, in the past, the vertical resolution of such data was limited to 0.5 to 1 meter because reducing thermistor calibration errors to a small fraction of the expected mean temperature difference between adjacent sensors is difficult.⁹

In conjunction with Analytic Information Processing, Incorporated, APL has developed a high-resolution thermal-gradiometer system that can be mounted on a vertical chain for horizontal towing, and it has added to the chain a high-resolution conductivity system. The combined temperature/conductivity system measures temperature to 5 centimeters vertical resolution and conductivity to 30 centimeters. With this instrument, long horizontal tows can be made during which sufficient data can be collected for a statistical characterization. In addition, the high-vertical-resolution temperature and conductivity measurements that are possible with the system can accurately characterize the vertical scales of SSA. Thus, the data obtained provide a good basis for statistically characterizing the two-dimensional geometric structure of the SSA field.

Because conductivity cells respond very quickly to changes in oceanic conductivity, they can sample temperature and salinity fluctuations on spatial scales as short as a few centimeters (assuming typical tow speeds up to 6 knots) and are usually the preferred instrument for investigating microstructure and oceanic turbulence. However, much insight can be gained by examining temperature fluctuations on slightly larger scales, because regions of enhanced SSA are naturally broadband, appearing both on high-frequency conductivity sensors and temperature sensors. In addition, the higher vertical resolution of the thermistor system can be used to characterize SSA structure to smaller vertical scales than can the conductivity system.

PATCH GEOMETRY AND ARRIVAL STATISTICS

Analysis Techniques

To characterize the relative abundance and geometric structure of episodes of excess SSA (patches) from temperature data, it is necessary to develop a methodology for detecting patches on horizontally towed single sensors, and then for combining patches detected on different sensors to form an aggregate or cluster of patch detections. The methodology used in accomplishing these two tasks is described below.

The concept of patch detection can be generally described as follows. Towed arrays of temperature sen-

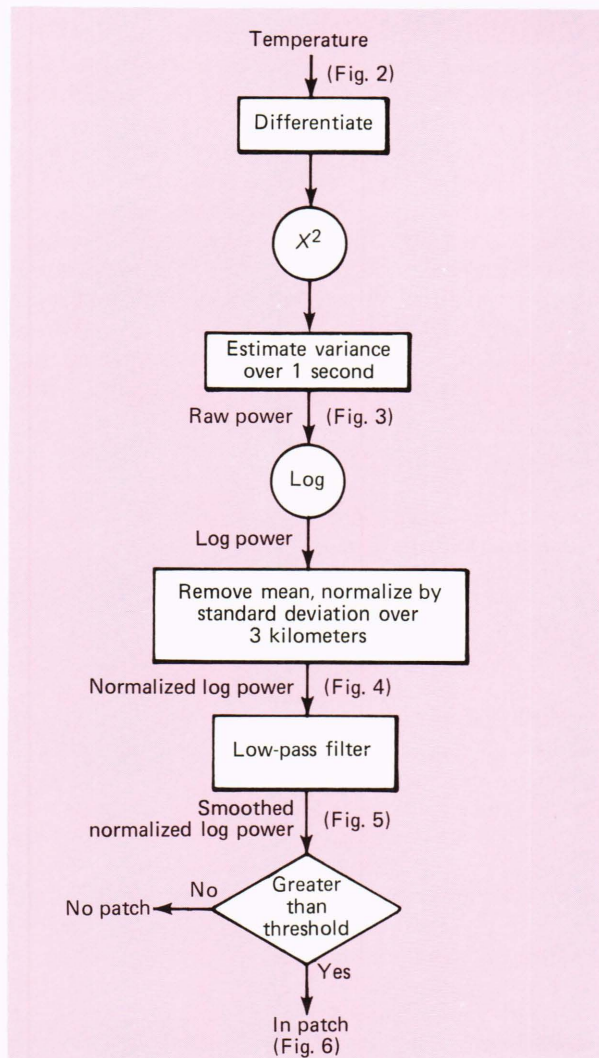


Figure 1—A schematic of patch detector processing. Temperature data are differentiated horizontally, thereby emphasizing short fluctuation scales. The variance is calculated over 1-second intervals followed by a logarithmic transformation. The resulting log power is normalized to zero mean and unit variance using the surrounding 3 kilometers of data. The data are low-pass filtered and compared to a threshold. Note that these calculations are made separately for each sensor in the array. Figure numbers refer to examples of data at the indicated stage of the processing.

sors (thermistors) produce a two-dimensional plane of measurements defined in the vertical by the depth interval spanned by the sensors and in the horizontal by the length of the tow. The object of patch detection is to divide the plane of data into regions of two types: regions with high SSA and regions with low SSA. The objective can be accomplished by relevant processing of each individual thermistor time series to produce a variable that indicates the level of SSA. The variable is subsequently compared to a threshold to divide the data into two categories: high SSA (patches) and low SSA (no patches).

Figure 1 illustrates the processing of thermistor data and the detection of patches; each sensor in the array is processed independently. Because high-frequency temperature fluctuations are the signature of turbulent events in the ocean, the temperature data are differentiated horizontally to emphasize the high-frequency fluctuations. Wavenumber, the reciprocal of wavelength, is a measure of the spatial frequency associated with the signal and is measured in cycles per meter. Throughout this article, the assumed value of the tow speed will be 3 meters per second. Assuming a constant tow speed means that high temporal frequencies are synonymous with high spatial frequencies or wavenumber. The spectrum of temperature in the ocean exhibits decreasing power with increasing wavenumber; typically, the spectrum is proportional to k^{-2} to $k^{-2.5}$, where k is the horizontal wavenumber. Differentiating the data horizontally effectively mul-

tiplies the spectrum by k^2 , producing a nearly flat spectrum with equal contributions from all scales.

After differentiation, the raw level of SSA is quantified by calculating the variance over 1-second (or 3-meter) nonoverlapping blocks. Figure 2 is a raster plot of the temperature prior to differentiation. Figure 3 is the variance of these data after differentiation; this quantity will be referred to as raw power. Figure 3 clearly shows regions of enhanced SSA surrounded by regions of relatively quiet data. Note that the power within the enhanced regions exhibits a high degree of internal variation (intermittency), often orders of magnitude. Also, note that at this 10-centimeter vertical resolution, regions of high SSA often span a number of sensors.

Continuing with Fig. 1, the log of raw temperature power data is calculated, and the result is termed log power. The purpose of this step is to symmetrize the probability density function of the SSA indicator. It also serves to compress the data in amplitude so that subsequent filters can operate more effectively. The log power data are then normalized to zero mean and unit variance using the surrounding 3 kilometers of data, which ensures that the resulting data are statistically stationary (at least through second order) by removing long-scale variations in SSA levels. Figure 4 is a histogram of the normalized log power; the data exhibit a near-Gaussian distribution function, implying that the original raw power follows a roughly log-normal distribution. This property of the variance of

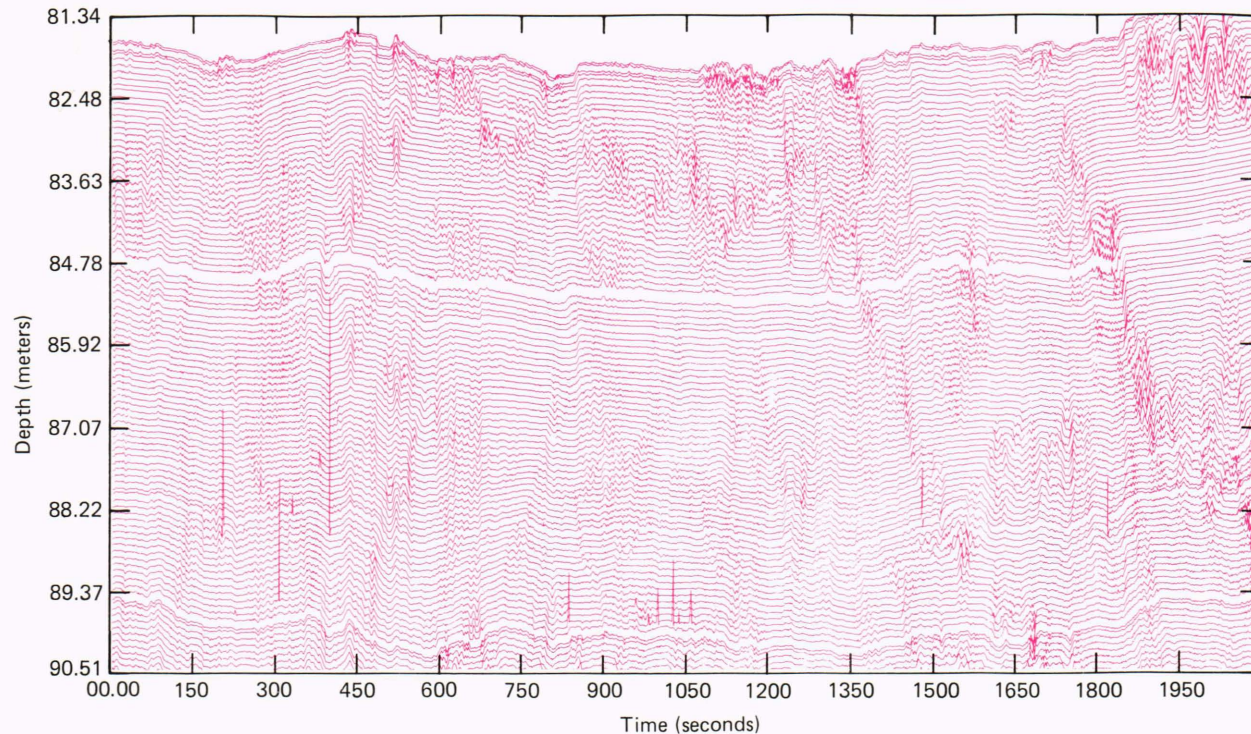


Figure 2—A 32-minute segment of thermistor data taken in the seasonal thermocline of the Sargasso Sea in November 1982. Every second thermistor is plotted for a total of 100 sensors. The horizontal scale is 150 seconds per division corresponding to 435 meters at 2.9 meters per second tow speed. The vertical scale represents depth. The first point in each thermistor time series is plotted at the depth of that sensor, and subsequent points are plotted relative to the first using a scale of 0.5°C per vertical division. Note areas of high-frequency temperature fluctuations spanning a number of sensors vertically.

temperature derivatives has been observed by a number of investigators.^{4,5}

As stated previously, we wish to divide the data into regions of high and low SSA. This is easily accomplished by comparing the normalized log power to a threshold, chosen so that only a relatively small fraction of the data exceed the threshold and are thus characterized as patches. Such a procedure applied at this stage would produce many closely spaced, short, apparent patches resulting from the internal intermittency within true patches. To avoid this situation, the normalized log power is smoothed using a low-pass filter whose cutoff wavelength is 50 to 200 meters. Figure 5 is a gray-scale representation of the data after they are smoothed using a 100-meter window. Regions that are on the order of 100 meters and larger have been emphasized, and much of the internal intermittency within patches has been removed.

Figure 6 is a representation of the data in patch form produced by comparing the data of Fig. 5 to a threshold, in this case 0.8. The normalized log power is dimensionless. Each single-sensor patch is represented as a rectangle whose horizontal dimension is the length of the region with data greater than the threshold, and whose vertical dimension is determined by the sensor spacing. Clearly shown are vertically contiguous regions of single-sensor patches extending over many sensors. For example, the large group of single-sensor patches near 300 seconds is about 6 meters high and 650 meters in total width.

One simple method of combining single-sensor patches into multiple-sensor patch groups objectively is to define a patch group as a spatially contiguous set of patches; i.e., two single-sensor patches on adjacent sensors are grouped together if they overlap horizontally. Throughout the rest of this article, a patch will be considered a single-sensor event and a patch group, or simply a group, as a multiple-sensor contiguous set of patches. Figure 7 is a schematic of a hypothetical group of five patches. Illustrated are some simple descriptions related to the geometry of a given patch group: height, width, and group slope.

In addition to these descriptors of group geometry, three measures of the relative abundance of patches will be considered. The patch arrival rate and group arrival rate are defined as the number of patches and groups (respectively) per sensor per kilometer. The average intermittency is the fraction of data classified as a patch by the patch detector. This is not to be confused with the internal intermittency within a patch; it is a measure of the overall "patchiness" of the data.

Analysis Results

The methodology described above has been applied to 200 kilometers of towed thermistor data taken in the seasonal thermocline of the Sargasso Sea in November 1982. Noise limitations and calibration accuracy of the towed chain instrument system are discussed elsewhere.⁹ Data were processed from 200 thermistors spaced vertically at 5-centimeter intervals. The thermis-

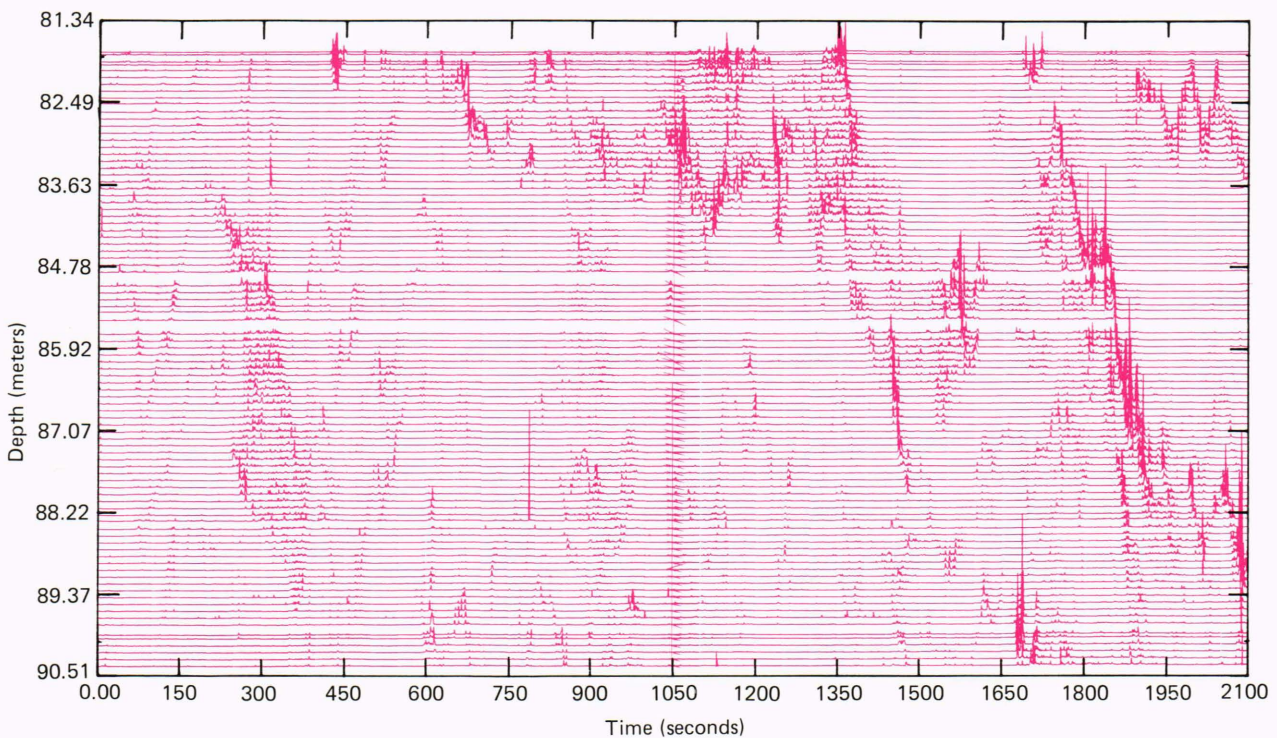


Figure 3—A plot of the raw power over the same time segment as Fig. 2. The data have been differentiated horizontally, and the mean square (or variance) has been calculated over 1-second (3 meters at 3-meters-per-second tow speed) intervals. Notice how regions of small-scale temperature fluctuations have been enhanced. For example, the region of activity in the vicinity of 300 seconds is more visible on this plot than in Fig. 2.

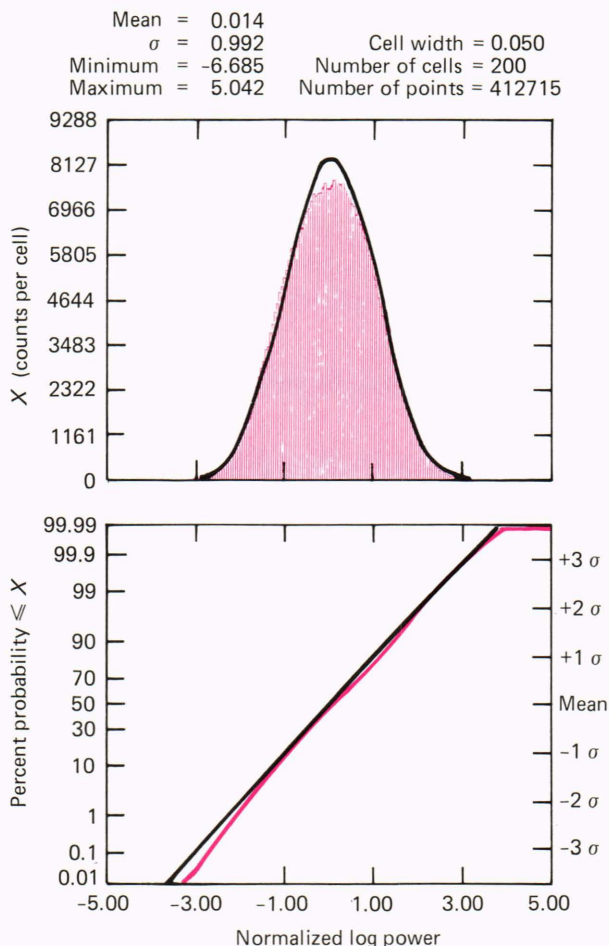
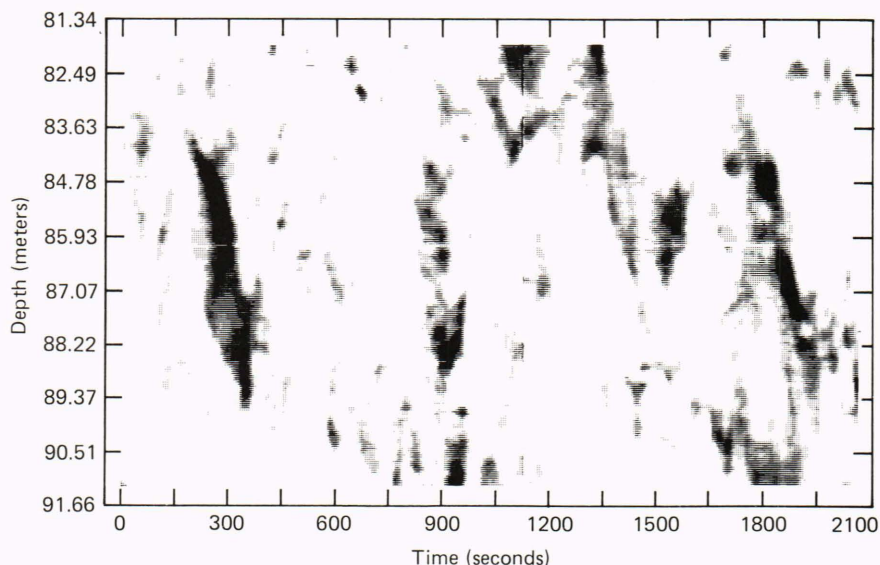


Figure 4—A histogram and cumulative distribution function of normalized log power for the same data segment as Figs. 2 and 3. This figure represents the form of the data after log transformation of the raw power and normalization to zero mean and unity variance. The black line is a Gaussian distribution with the same mean and variance and indicates that the data (in log power) are approximately Gaussian. This observation implies that the raw data are roughly log normal, a property of temperature-derivative variance noted by others.^{4,5}

Figure 5—A gray-scale representation of the normalized log power after low-pass filtering with a 100-meter cutoff. Only values above 0.6 are shaded; darker regions represent greater intensity of fluctuations. Notice how the tall regions of intense small-scale activity correlate with similar regions in Figs. 2 and 3. The normalization has emphasized the region of activity near 300 seconds.



tors were processed using a 5-hertz bandwidth, thereby including horizontal fluctuation scales as short as 60 centimeters at 3-meters-per-second tow speed.

The data were processed using 12 different combinations of filter cutoff and threshold in the patch detector. Analysis results, especially arrival statistics, are in general a function of these two parameters. Because the level of the SSA indicator (log power) has been normalized by the local statistics and further modified by the final low-pass filter, it is not possible to predict the arrival statistics prior to processing the data for patches. Arrival statistics and single-sensor patch-length statistics were computed after applying the patch detection methodology. Variations of the arrival statistics were examined as functions of threshold and filter cutoff.

From least-squares fits to the data, it has been determined that the patch and the group arrival rates and the average intermittency can be described by simple functions of filter cutoff wavelength, λ , and threshold.¹⁰ Both the patch and the group arrival rates are inversely proportional to λ and decrease exponentially with increasing threshold. The average intermittency varied similarly with threshold but was inversely proportional to $\lambda^{1/2}$. Because the average intermittency equals the patch arrival rate times the average length of a single-sensor patch, the average patch length is proportional to $\lambda^{1/2}$ and exponentially decreases with threshold. The effect of increasing λ is to further correlate those data just prior to thresholding, implying that, for a given amount of data, the number of independent “chances” for a patch arrival is inversely proportional to the correlation distance. In turn, the correlation distance is proportional to the filter wavelength cutoff. The average intermittency is less sensitive to λ . This relationship exists because, although there are fewer patches per kilometer as λ is increased, the patches themselves become longer.

Most of the results of the statistical analysis of patch group geometry cannot be summarized simply as a

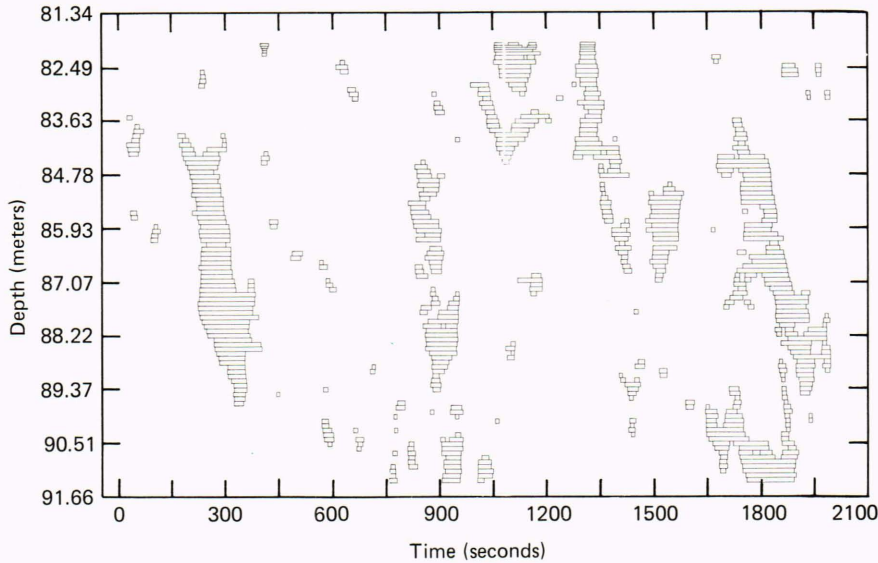


Figure 6—A patch representation of the data of Figs. 2, 3, and 5. The data of Fig. 5 are compared to a threshold (0.8 in this case), and a rectangle is plotted on that sensor over the time period where the threshold is exceeded. The height of each rectangle is two sensor spacings (10 centimeters); for clarity, only every second thermistor is plotted. Notice how single-sensor patches cluster into groups. Also notice how groups of patches often cluster together; these may, in fact, be part of a larger cluster whose internal intermittency makes them appear separate.

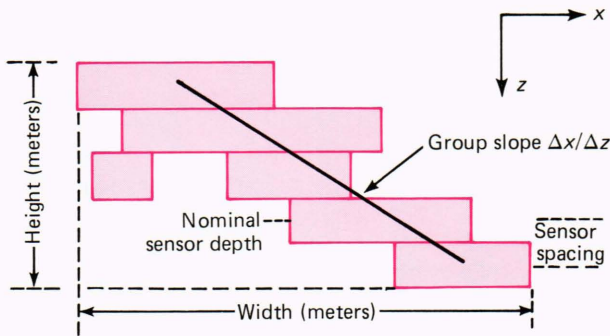


Figure 7—A schematic of patch-group geometric descriptors. Patch-group heights and widths are extremes of the vertical and horizontal extent of the group. The group slope is taken between the centers of the top and bottom single-sensor patch.

function of patch-detector operating parameters. The results presented below are for a single combination of λ and threshold and are representative of other combinations of these parameters. The specific case chosen is λ equal to 100 meters and threshold equal to 1.0. With these parameters, only a small fraction—6.9 percent—of the data are considered by the detector to be in patches. The single-sensor patch arrival rate is $0.67 \text{ (sensor-kilometer)}^{-1}$ or on the average, two patches every 3 kilometers on each sensor.

Figure 8 is a plot of the heights and widths of roughly 1000 patch groups. Note that the definition of a patch group admits the possibility of a single sensor “group.” The vertical resolution of the thermistor chain is responsible for the banding of groups at 5-centimeter height intervals. The scales of this plot have been adjusted so that groups whose width-to-height ratio is 100 fall along the diagonal line. However, in this case, most of the groups have a width-to-height ratio greater than 100. A least-squares fit of the width to the height results

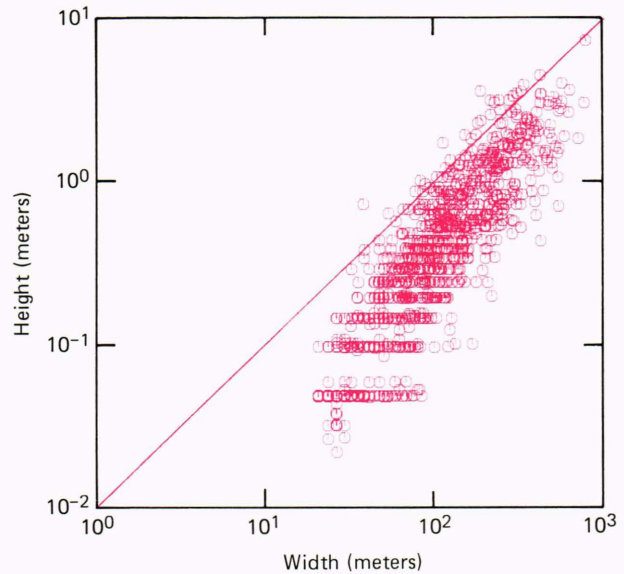


Figure 8—A scatter plot of group heights and widths for roughly 1000 groups. The scales have been adjusted so that groups whose width-to-height ratio is 100 fall on the diagonal line. Most groups fall below the line; the mean aspect ratio is about 200. These results and those that follow are for a low-pass filter cutoff of 100 meters and a threshold of 1.0.

in an average aspect ratio of about 200. The value of 200 is consistent with prevailing evidence that structures in the ocean are on the order of 100 times larger in the horizontal than in the vertical. The heights and widths are moderately well correlated (correlation coefficient 0.81), indicating that the data may be adequately characterized by a single mean aspect ratio. However, we see that as the patch group height decreases, the width does not fall off as rapidly. This may be a manifestation of gravitational collapse where a well-mixed patch with a given mean density collapses in the vertical, spreading horizontally, in order for the

fluid in the patch to reach its equilibrium depth in the density-stratified thermocline.

Figure 9 is a histogram of the group height showing the relative abundance of patch groups as a function of group height. The histogram cell size was chosen as one nominal sensor spacing (5 centimeters), and the scales were adjusted so that multiples of the sensor spacing fall in the center of a cell. The black line is an estimated exponential distribution with the same mean and variance as the observed data.

Only 17.8 percent of the groups are comprised of a single patch. However, 61.3 percent of the observed patch groups are shorter than 0.5 meter. This observation of the relative abundance of small groups implies that conventional towed array systems with 0.5-

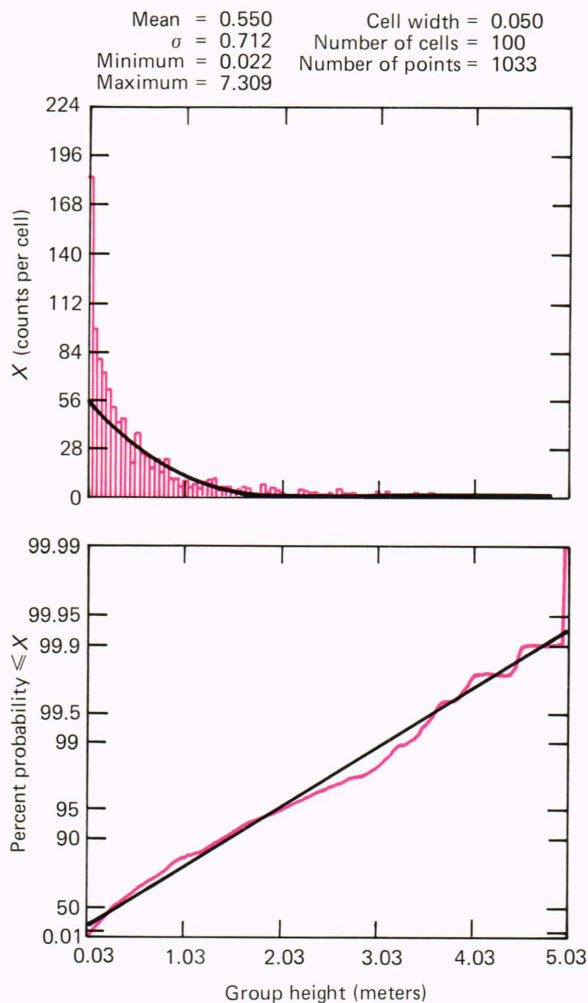


Figure 9—A histogram and cumulative distribution function of the group height. The black line is an estimated exponential distribution with the same mean and variance as the data. A large fraction of the groups (95 percent) is less than 2 meters high. The median group height is only 30 centimeters, indicative of how small many of the groups are. The standard deviation is greater than the mean, indicative of a large variation in group size. There appears to be no preferred group height since the distribution appears to be relatively continuous.

to 1-meter sensor spacings are inadequate to resolve the vertical scales of SSA.

The distribution of patch group heights is roughly continuous, implying that there exists no preferred vertical scale for patches of turbulent activity. The mean vertical height is 55 centimeters and the standard deviation is 71 centimeters. The fact that the standard deviation is greater than the mean confirms the observation apparent from Fig. 8: patch groups show a large variation in vertical scales.

The relative abundance of patch groups whose heights are only a few centimeters may be due to the remaining intermittency within larger groups. That is, a number of the smaller groups observed may, in fact, be part of the edges of larger groups; their separation from the main group may be only a consequence of the intermittency of the group near its boundaries. In Fig. 6, for example, we can see a fair number of 10- to 20-centimeter groups located suspiciously close to larger groups. This observation suggests that perhaps a more sophisticated grouping algorithm is required, one that does not require patches to overlap on adjacent sensors.

The general appearance of the histogram of patch heights is similar to that observed by Dillon,⁶ whose measurements were made with a vertical microstructure profiler. For the oceanic data he analyzed (some data from a freshwater lake were also considered), the average height of a microstructure patch is 44 centimeters with a standard deviation of 23 centimeters. These averages were computed over only 56 patches. The values are roughly consistent with the results presented here, although both mean and standard deviations are a little smaller in Dillon's data. This may be a result of the microstructure profiler intersecting only a portion of tall patches that have been tilted (or sheared out) by horizontal currents that vary with depth, an effect that will be discussed in more detail below.

Figure 10 quantifies the relative abundance (or arrival rate) of patch groups as a function of their height. The conditional group arrival rate is the number of patch groups per kilometer in a 10-meter aperture whose height is greater than a specified value. For example, on the average, groups larger than 2 meters in height arrive only once in 2 kilometers of tow. Groups larger than 3 meters arrive only once in about 10 kilometers. Patch groups with heights from 1 to 3 meters and widths of a few hundred meters are consistent with the generation mechanisms of salt-fingering and shear instabilities.⁷ Mixing events extending over larger vertical scales than about 3 meters appear to be relatively rare. However, caution should be exercised in drawing such a conclusion based on the limited 10-meter aperture of the array. For example, a patch group that appears to be 4 meters tall may be only the top (or bottom) 4 meters of a taller patch. The slight discontinuity of the conditional group arrival rate in the neighborhood of 3 meters may be a manifestation of the limited aperture of the array. The relative abundance of groups whose heights are greater than a small fraction (say 30 percent) of the array aperture is par-

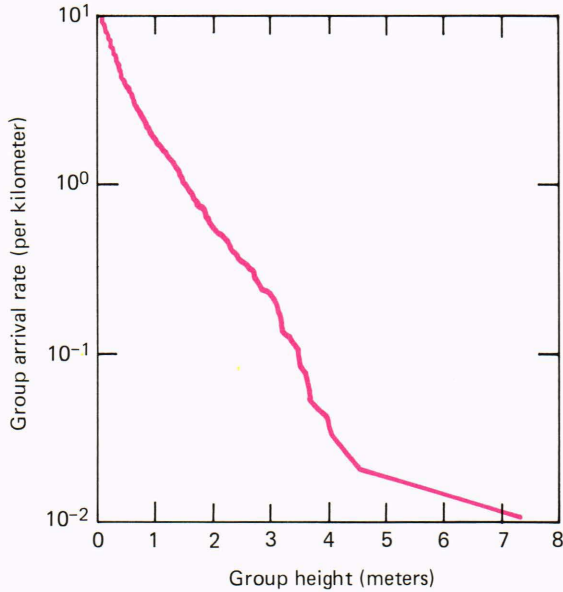


Figure 10—The conditional group arrival rate, defined as the number of patch groups per kilometer in a 10-meter aperture whose height exceeds a particular value. This is a method of quantifying the relationship between geometry and the abundance of the patch groups. For example, groups whose height exceeds 2 meters arrive, on the average, once in 2 kilometers of data.

ticularly susceptible to misinterpretation.

Figure 11 is a histogram of the patch group widths. Since the group height and widths are well correlated, the relative abundance of horizontally short groups is not surprising. About 90 percent of the groups are less than 250 meters long. The average is about 120 meters but, just as in the case of group heights, the group width exhibits a wide variety of horizontal scales, from 20 meters to 1 kilometer.

Figure 12 is a histogram of the group slope, a quantity defined by Fig. 7. The distribution is essentially zero mean with a standard deviation of 122, and it appears more peaked than the overplotted Gaussian distribution function of the same mean and variance. A patch group that is vertically aligned at its generation time will tilt under the action of a large-scale current that changes with depth. After a time t , the slope of the patch group will be $S \cdot t$, where S is the derivative of the horizontal current with respect to depth (the current shear) over the vertical scales of the patch. The action of vertical shear with time may account for the observed group slopes.

The value of the standard deviation of group slope is suggestive of the possible influence of internal waves. Typical root-mean-square slopes of long wavelength (> 100 meters) internal waves are on the order of 100 to 200, which suggests the possibility that many of the patch groups may lie along curves of constant density that have been tilted by internal wave displacements.

Patch heights determined by dropped measurements can cause the actual height of the patch to be underestimated, particularly when the patches have been tilted

Mean = 120.682
 σ = 115.647 Cell width = 31.741
 Minimum = 20.358 Number of cells = 31
 Maximum = 1004.343 Number of points = 1033

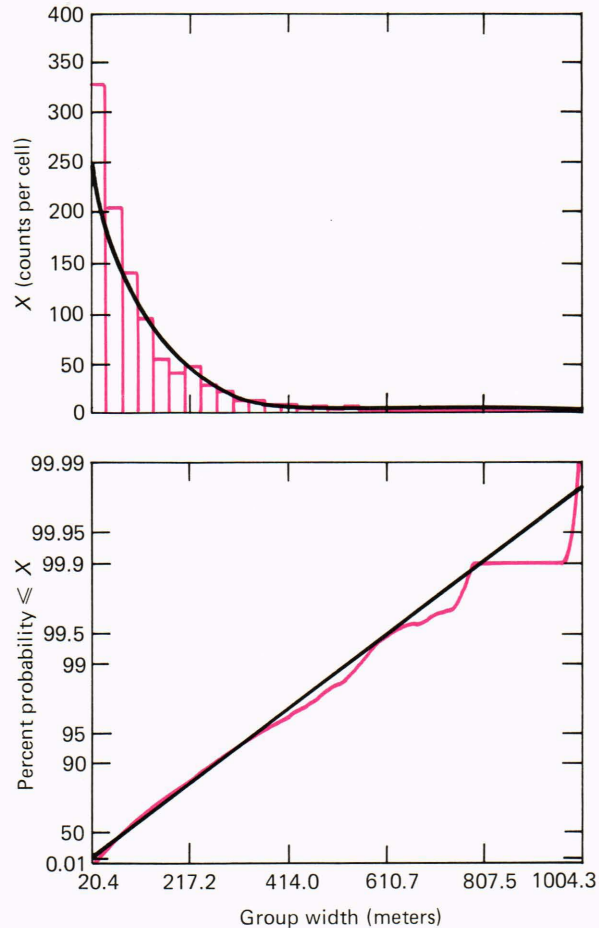


Figure 11—Histogram and cumulative distribution of patch-group widths. The black line is an estimated exponential distribution having the same mean and variance as the observations. Most of the groups are relatively short; 90 percent are less than 250 meters long, although considerable variation is evident.

by shear. This underestimate can result because the instrument may go through only a small part of the patch. Measurements of patch heights by towed instrument systems with low vertical resolution can also be complicated by significant group slopes. For example, two single-sensor patches on adjacent sensors spaced 3 meters apart may or may not be part of the same patch, particularly if the patch is highly skewed by the action of current shear. Using high-resolution towed data avoids these problems by adequately resolving the vertical and horizontal scales of fluctuations in SSA.

CONCLUSION

The results presented here are from a preliminary investigation of the geometry and arrival statistics of patches of SSA. The observed geometry of the patches is consistent with a number of mechanisms that generate SSA in the ocean, such as shear instabilities and

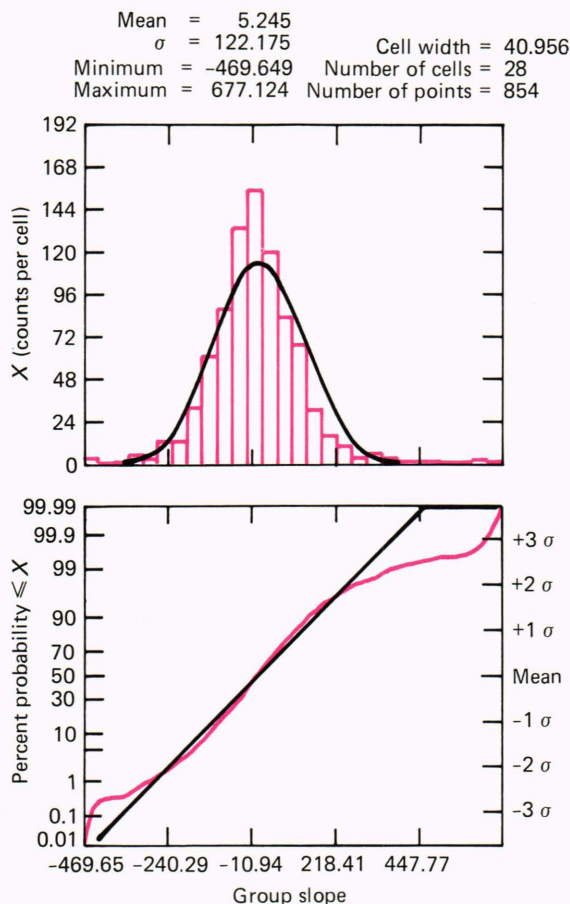


Figure 12—Histogram and cumulative distribution functions of group slope. The data are essentially zero mean with a standard deviation of 122 and are more peaked than the overplotted Gaussian distribution, which has the same mean and variance as the data.

double diffusive phenomena. Insight into the relative importance of these generation mechanisms can be enhanced by combining observations such as these with simultaneous (or near-simultaneous) measurements of current shear, ambient temperature and conductivity profiles, and estimates of internal wave displacements. For example, vertical profiles of conductivity and temperature permit one to predict the depth intervals over which salt-fingering is likely to occur.⁷ Correlations

THE AUTHOR

HOWARD C. SCHOEBERLEIN is a physicist with the Hydrodynamics Group of the Submarine Technology Department. Born in Baltimore in 1953, Mr. Schoeberlein obtained a B.S. in physics from Towson State University in 1975, followed by an M.S. in physics from Drexel University in 1977 and an M.S.E.E. degree from The Johns Hopkins University APL Education Center in 1984. After a two-year teaching assistantship at Drexel, Mr. Schoeberlein joined APL in 1977 as an associate physicist. His professional interests include digital signal processing, time series analysis, probability, and stochastic processes, with particular emphasis on applying these techniques to the analysis of small-scale oceanographic data. He is currently exploring the connection between patches of small-scale turbulent activity and larger scale internal waves. He is a member of Sigma Pi Sigma, the national physics honor society.

between these regions and regions where SSA is observed may provide insight into the relative importance of salt-fingering as a generation mechanism. Correlations between regions of high shear or internal wave slope and regions of active SSA may provide clues to the relative importance of shear instabilities as a source of oceanic turbulence. Correlations between internal wave slope and the slope of patch groups may also provide insight into this generation mechanism.

Although the results presented here are preliminary, they serve to demonstrate the utility of high-density towed arrays, as well as the analysis techniques described here, in studying small-scale turbulent activity in the ocean.

REFERENCES and NOTE

- 1 T. R. Osborn and C. S. Cox, "Oceanic Finestructure," *Geophys. Fluid Mech.* **3**, 321-345 (1972).
- 2 T. R. Osborn and L. E. Bilodeau, "Temperature Microstructure in the Equatorial Atlantic," *J. Phys. Oceanogr.* **10**, 66-82 (1980).
- 3 M. C. Gregg and T. R. Sanford, "Signatures of Mixing from the Bermuda Slope, the Sargasso Sea, and the Gulf Stream," *J. Phys. Oceanogr.* **10**, 105-127 (1980).
- 4 M. C. Gregg, "Microstructure Patches in the Thermocline," *J. Phys. Oceanogr.* **10**, 915-943 (1980).
- 5 D. T. Georgi and R. W. Schmitt, "Fine and Microstructure Observations on a Hydrographic Section from the Azores to the Flemish Cap," *J. Phys. Oceanogr.* **13**, 632-647 (1983).
- 6 T. M. Dillon, "Vertical Overturns: A Comparison of Thorpe and Ozmidov Length Scales," *J. Geophys. Res.* **87** (C12), 9601-9613 (1982).
- 7 S. A. Mack, D. C. Wenstrand, J. Calman, and R. C. Burkhardt, "Characteristics of Thermal Microstructure in the Ocean," *Johns Hopkins APL Tech. Dig.* **3**, 28-35 (1982).
- 8 M. C. Gregg, "Finestructure — Oceanic Kinks and Wiggles," *Nav. Res. Rev.* **3**, 52-72 (1982).
- 9 D. C. Dubbel, "The Reduction in Finestructure Contamination of Internal Wave Estimates from a Towed Thermistor Chain," *Johns Hopkins APL Tech. Dig.* **6** (1985).
- 10 Expressions and scalings for the group arrival rate (GAR), patch arrival rate (PAR), and average intermittency ($\langle I \rangle$) were determined from the data as a function of low-pass filter wavelength (λ) and threshold (T) by least-squares fits to the data. The results are

$$\begin{aligned}
 PAR &= \frac{0.530}{\lambda} 10^{-0.913T}, \\
 GAR &= \frac{0.0218}{\lambda} 10^{-0.611T}, \quad \text{and} \\
 \langle I \rangle &= \frac{0.425}{\lambda^{1/2}} 10^{-1.322T},
 \end{aligned}$$

where λ is in kilometers and T is dimensionless.

